International Journal of Nanoelectronics and Materials
IJNeaM
ISSN 1985-5761 | E-ISSN 2232-1535

Isothermal Oxidation Behaviour of Heat-treated Fe-33Ni-19Cr Series Ni-based Superalloy

Megat Farhan Nazmi Megat Mohamad Halim[a], Noraziana Parimin[a,b,*] and Esah Hamzah[c]

[a]*Faculty of Chemical Engineering & Technology, Universiti Malaysia Perlis (UniMAP), 02600 Arau, Perlis, Malaysia*
[b]*Surface Technology Special Interest Group, Faculty of Chemical Engineering & Technology, Universiti Malaysia Perlis (UniMAP), 02600 Arau, Perlis, Malaysia*
[c]*Faculty of Mechanical Engineering, Universiti Teknologi Malaysia (UTM), 81310 Skudai, Johor, Malaysia*
**Corresponding author. Tel.: +604-9798154; fax: +604-9798178; e-mail: noraziana@unimap.edu.my*

ABSTRACT

The impact of heat treatment on the high temperature oxidation of Ni-based superalloys, specifically the Fe-33Ni-19Cr series, is discussed in this study. This alloy, designated LT950 and HT1160, is heat treated at two distinct temperatures, 950 °C and 1150 °C, for three hours of soaking time, followed by a water quench. Rockwell hardness tests and optical microscopy were used to characterize the heat-treated samples. An isothermal oxidation test was performed on the heat-treated samples for 200 hours at 900 °C. The oxidation kinetics were ascertained by measuring the weight change of the oxidized sample. Oxidized samples were characterized by morphological analysis of the oxide scale using a scanning electron microscope (SEM) and oxide phase analysis using x-ray diffraction (XRD). As a result, the sample's grain size increases with increasing heat treatment temperature. The results of the Rockwell hardness test indicate that the Rockwell hardness number decreases as the heat treatment temperature rises. However, every heat-treated sample that was put through the isothermal oxidation test displayed a pattern of weight gain as the length of exposure increased. Because fine-grained LT950 has a lower parabolic rate constant, it indicates a lower rate of oxidation and therefore has good resistance to oxidation. XRD analysis shows that several oxide layers have formed on the surface of the oxidized sample consisting of Cr-containing oxides from the Cr_2O_3 and $MnCr_2O_4$ phases. SEM analysis of fine-grained LT950 showed uniform oxide scale, while coarse-grained HT1150 showed the formation of cracked and porous structures.

Keywords: *Fe-Ni-Cr series, Heat treatment, Isothermal oxidation, Ni-based superalloy, Oxidation kinetics*

1. INTRODUCTION

Superalloys are often used by engineers and metallurgists to describe a class of metal alloys intended to work at high temperatures [1]. This alloy can withstand an average temperature of 1050 °C with exposure to temperatures as high as 1200 °C, which is near the melting point of the material. In addition to their general strength, superalloys are renowned for their capacity to retain high strength and creep rupture resistance up to their high melting point. The foundation of these alloys is a face-centered cubic (FCC) matrix, which can withstand substantial alloying for strengthening and increased resistance to oxidation and other impacts from the environment [2].

One type of Ni-based superalloy is the Fe-33Ni-19Cr series. This alloy resists corrosion and oxidation at high temperatures and has exceptional mechanical qualities [3,4]. It is commonly used in power generation and heat processing applications involving high temperature exposure [5,6].

The Fe-33Ni-19Cr series Ni-based superalloy has a greater concentration chromium where acts as an oxide-forming element [3]. A high concentration of Cr, usually between 15 and 25 percent, causes the surface to form a slowly developing oxide scale of Cr_2O_3 [7,8]. The mechanical qualities and oxidation resistance of the alloy improve when the nickel content is higher than that of stainless steel. In general, the density of the scale and its capacity for adhering to the substrate at high temperatures have a significant impact on an alloy's resistance to oxidation. The oxide scale formed on the surface of the alloy acts as a protective barrier between the alloy and the environment.

Because the alloy and oxide scales have different thermal expansion coefficients, these alloys experience oxide exfoliation at high temperatures and over extended periods of service [9,10]. The protective layer of oxide that had previously developed on the alloy's surface has diminished as a result of this phenomenon. Further studies have been recorded to minimize oxide exfoliation such as shoot exfoliation, surface treatment and grain refinement. Grain modification from the heat treatment process is one of the suitable ways to refine the grain structure [11,12]. The heat treatment method successfully refined the alloy grain structure from our previous work [3,10,13]. A higher grain boundary area found in fine grain sizes serves as a fast diffusion path for metal ions to reach the alloy surface and quickly form an oxide scale. As a result, in this study, the alloy underwent a heat treatment process to alter its grain structure and size. This was followed by an isothermal oxidation test to examine how oxide scale forms on the alloy.

This study highlights the effect of different two heat treatment temperatures of Fe-33Ni-19Cr superalloy on isothermal oxidation test at 900 °C. The analysis also highlighted the effect on oxidation kinetics and phase analysis of the solution treated Fe-33Ni-19Cr superalloy after high temperature isothermal oxidation.

2. MATERIALS AND METHODS

The material used in this study is commercially available INCOLOY 800H from the Fe-33Ni-19Cr series Ni-based alloy. The composition of this material determined using an optical emission spectrometer in weight percent (wt%) is 33.0 Ni, 19.0 Cr, 0.078 C, 0.053 Al, 0.489 Ti, 0.001 S, 0.315 Si, 0.556 Mn, 0.082 Cu and the remaining Fe. The sample was cut to dimensions approximately 10 mm x 10 mm x 3 mm. The heat treatment process is performed at two different temperatures, which were 950 °C and 1150 °C for 3 hours of soaking time. The sample was immediately quenched in water. These samples are marked as LT950 and HT1150, respectively. The heat-treated samples were characterized in terms of grain size measurements using the ASTM E112 linear intercepts procedure and the Rockwell hardness tests.

Samples need to be ground first before undergoing the oxidation test. The grinding process is carried out using a grinding machine and silicon carbide (SiC) paper. SiC paper is used with grit sizes ranging from P180 to P600. The weight and dimensions of the sample were recorded after the sample went through the grinding process. Analytical balances are used for weighing operations and vernier calipers are used to obtain dimensional measurements. Oxidation tests are performed to determine oxidation behavior. This test is carried out isothermally at a temperature of 900 °C. In this study, a muffle furnace was used for high temperature oxidation. A quartz boat is used as a sample holder. The samples were subjected to the oxidation process in a furnace, followed by weight evaluation every 25 hours up to a total time of 200 hours. Oxidation kinetic graphs were plotted from the data of weight change for each interval exposure period.

Using x-ray diffraction (XRD) methods, the phases contained in oxidized samples were identified. The sample was exposed for 200 hours, and an XRD analysis was done to find out which oxide phase had formed. A scanning electron microscope (SEM) was employed to examine the structure of the oxide scale that developed on the alloy's surface. Samples exposed for 100 and 150 hours were subjected to SEM analysis to see the oxide phase that had developed on the alloy's surface. In this analysis, exposures of 100 and 150 hours were chosen in accordance with the oxidation kinetic pattern.

Equation (1), where x is the change in weight per surface area, t is the time, and c and m are constants, is used to compute the oxidation rate law. When m equals 1 or 2, it denotes a linear rate law or a parabolic rate law, respectively. For analytical purposes, m is set in a range of values; that is, the linear rate law is represented by a value of m between 0.50 and 1.49, and the parabolic rate law is represented by a value of m between 1.51 and 2.49. Equation (2) can be used to determine the parabolic rate constant, K_P. Equation (3) can be used to calculate the linear rate constant, K_L.

$$\log x = \left(\frac{1}{m}\right) \log t + c \quad (1)$$

$$x^2 = K_p t + c \quad (2)$$

$$x = K_L t + c \quad (3)$$

3. RESULTS AND DISCUSSION

3.1. Heat treatment

The determination of the average grain size was carried out as shown in Figure 1. Grain size calculations were measured by averaging grain diameters based on at least five optical micrographs using the ASTM E112 linear intercept procedure. The results show that increasing the heat treatment temperature will increase the grain size. The LT950 sample, heat-treated at 950 °C, recorded a fine grain size of 81.41 µm, while the HT1150 sample, heat-treated at 1150°C, recorded a coarse grain size of 166.12 µm. This result is different from the hardness test, which shows a pattern of decreasing hardness values when the heat treatment temperature increases as shown in Figure 1. The LT950 sample showed the highest hardness value of 81.04 HRB compared to HT1150 sample which is 69.06 HRB. As a result, increasing the heat treatment temperature has decreased the hardness value. These results prove that if the heat treatment temperature of the sample increases, the grain size increases and the hardness of the sample decreases. These findings, which show that grain size increases with heat treatment temperature, are in line with earlier research [11,12,13].

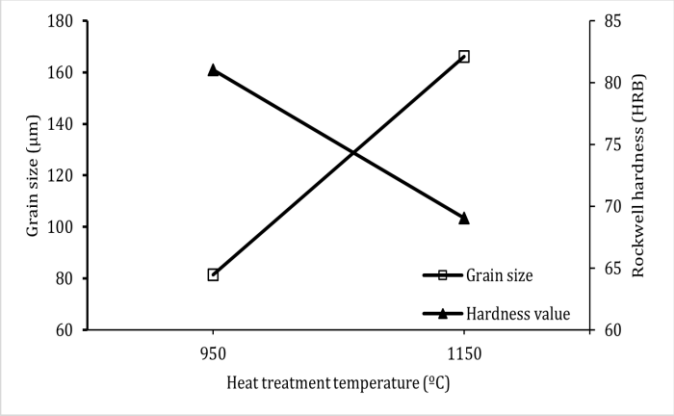

Figure 1. The effect of heat treatment on grain size and hardness.

3.2. Isothermal oxidation

All samples heat-treated from 950 °C and 1150 °C that underwent oxidation at 900 °C were included in the calculation for the determination of oxidation kinetics. By

dividing the weight change of each sample by its unique surface area, oxidation kinetics were computed. The weight change graph over time for each surface area is displayed in Figure 2. The graph demonstrates how the weight value changes as the oxidation time increases. Similar findings have been recorded by other researchers regarding the pattern of weight gain during prolonged exposure to high temperature conditions [3,4,10].

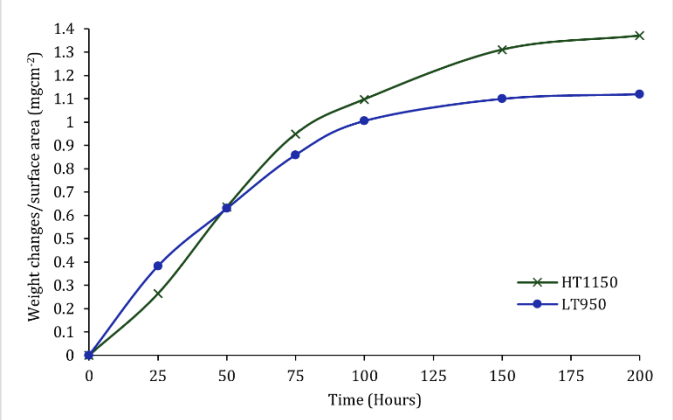

Figure 2. Oxidation kinetic.

The determination of the oxidation rate law was determined from the graph for the log of weight changes over surface area versus the log of time in hours shown in Figure 3. This graph is very important because it analyzes the type of oxidation rate of the samples tested in this research. The value of the constant, m as stated in equation (1) obtained from the graph in Figure 3 seat between 1.3 to 1.9 for HT1150 and LT950, respectively. These results show that the HT1150 follows a linear rate law, while the LT950 follows a parabolic rate law.

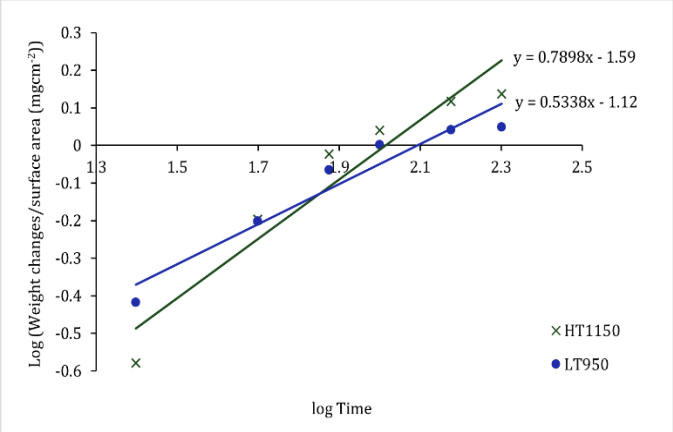

Figure 3. Oxidation rate law.

The parabolic rate constant for LT950 is determined using equation (2) as plotted in Figure 4. The parabolic rate constant of LT950 is 1.79 x 10^{-6} $mg^2cm^{-4}s^{-1}$. Since the oxide growth rate in this study is governed by a diffusion-controlled mechanism, a parabolic rate constant is preferred. This mechanism will cause oxide growth to slow down as exposure time increases. This is due to the development of protective oxide behavior that prevents further oxide scale formation. The oxide will act as a protective layer on the surface of the alloy that will stop the massive growth of oxide, thus enhancing the oxidation resistance.

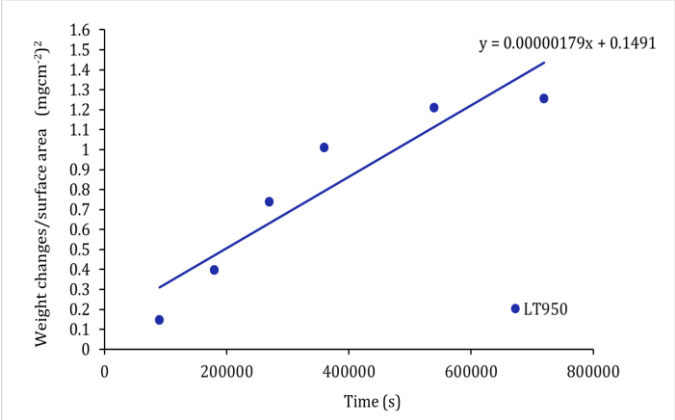

Figure 4. Parabolic rate constant.

As seen in Figure 5, a graph based on equation (3) was plotted to find the linear rate constant for HT1150. This result shows that the coarse grain size of heat-treated samples at 1150 °Cexperienced a higher oxidation rate that recorded a linear rate constant of 1.66 x 10^{-6} $mgcm^{-2}s^{-1}$. This results from the extensive oxide scale that forms during the oxidation process. The alloy's surface keeps developing an oxide scale as the oxidation time is extended, creating an oxide layer that serves as a barrier between the metal alloy and the environment, enhancing the alloy's protection. This phenomenon will be represented by a linear rate law, indicating the formation of oxide scale continues to grow as the duration of the oxidation test increase. These results indicate that the fine grain size (for LT950) of this alloy has recorded optimal oxide growth with a lower oxidation rate.

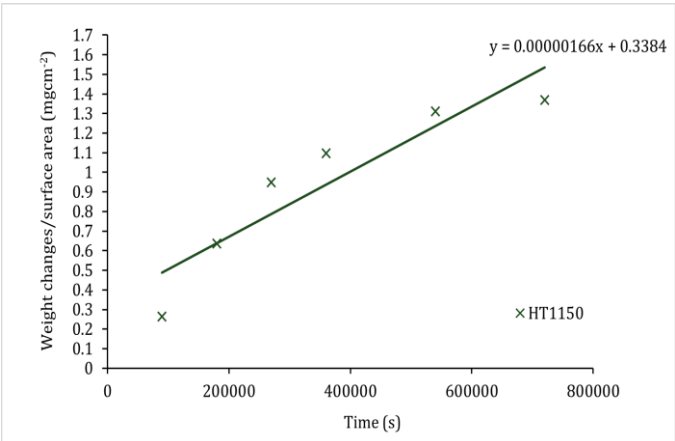

Figure 5. Linear rate constant.

Figures 6 and 7 represent the XRD test results for the LT950 and HT1150 samples after going through the oxidation test at 900 °C for 200 hours. The main phase observed that has a high intensity peak is the base metal label as Fe-Ni-Cr. During XRD analysis, a high intensity peak was found on the sample's surface, indicating the formation of a thin oxide layer.

Two main Cr containing oxides have been formed consisting of oxide phases Cr_2O_3 and $MnCr_2O_4$. The incorporation of Mn elements into Cr improves the protective behavior of Cr oxides. This is due to the rapid diffusion of Mn in Cr_2O_3 oxide [7,9]. Because this oxide will lessen the formation of volatile Cr species at high temperatures, the formation of a Mn-Cr spinel layer will positively impact the formation of oxide scale [8,14].

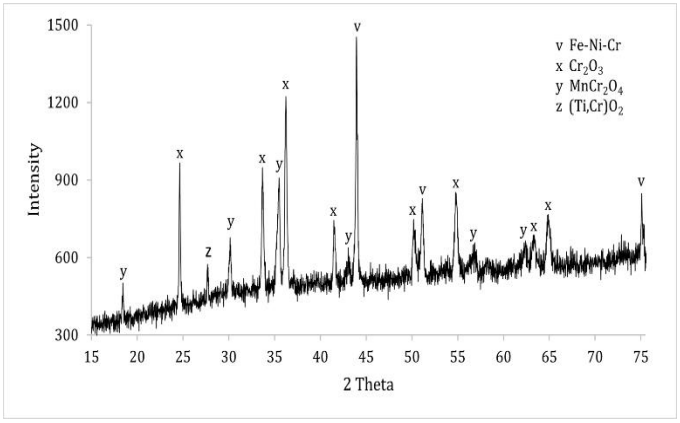

Figure 6. XRD analysis of LT950 samples.

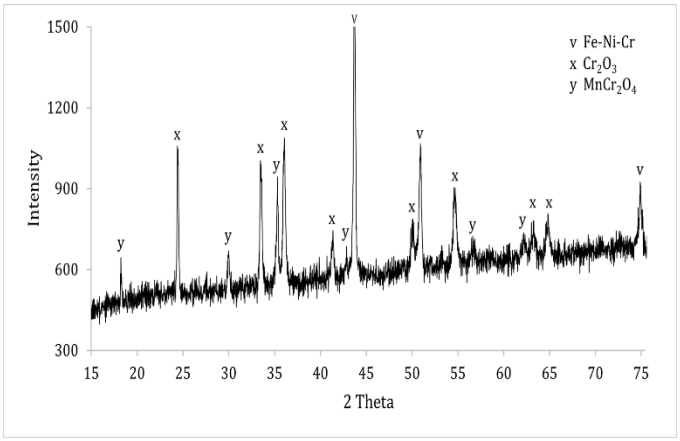

Figure 7. XRD analysis of HT1150 samples.

The main finding in the XRD analysis is the detection of the Ti-Cr oxide phase on the LT950 sample. The peak at 27.5° (110) verified the presence of this oxide. According to some reports, the production of Ti-rich oxide significantly affects oxidation protection and decreases oxide exfoliation [9,10]. It is believed that the creation of Ti-Cr rich oxide lessens the impact of Cr evaporation because $(Ti,Cr)O_2$ has a lower vapor pressure than Cr_2O_3 oxide [9]. The formation of this peak is consistent with the oxidation kinetics of this sample which shows a parabolic rate constant indicating a controlled oxide growth mechanism that forms a protective oxide scale. The formation of Ti-Cr oxide will reduce the oxidation rate to increase the optimum oxide thickness on the surface, thus following the parabolic rate law. Previous studies have successfully investigated the formation of Ti rich oxide, demonstrating a positive impact on the alloy's oxidation resistance [10].

On the other hand, the formation of Ti-Cr rich oxides on the HT1150 sample was not detected. This observation indicates that the Ti-Cr rich oxide formed on the surface of fine-grained LT950 has a protective behavior that can control the oxide growth rate to increase the optimum oxide thickness, thereby following a parabolic rate constant. This phenomenon does not occur in the coarse-grained HT1150 sample which records a linear rate law. A linear rate law indicates that the rate of oxide growth continues to increase as the exposure period is prolonged.

Oxidized LT950 and HT1150 sample were further analyzed using the SEM method to further examine the morphology of the oxides formed on the alloy surface. Analysis was performed at exposure periods of 100 hours and 150 hours based on the oxidation kinetic patterns at that time showing a steady state pattern for the LT950 sample and a significant increase pattern for the HT1150 sample. Figure 8 shows SEM images of both samples after isothermal oxidation test for 100 hours. Meanwhile, Figures 9 and 10 show SEM images of LT950 and HT1150 samples after exposure to isothermal oxidation for 150 hours, respectively.

SEM images for LT950 and HT1150 samples after 100 hours of exposure are shown in Figure 8 showing uniform and incessant oxide scale formation. As observed, there is the formation of network-like oxide structures such as grain boundary paths. Because of the higher diffusion rate that predominates in the grain boundary region, which acts as a short-circuit diffusion that promotes the formation of oxide scales, network-like oxides are formed.

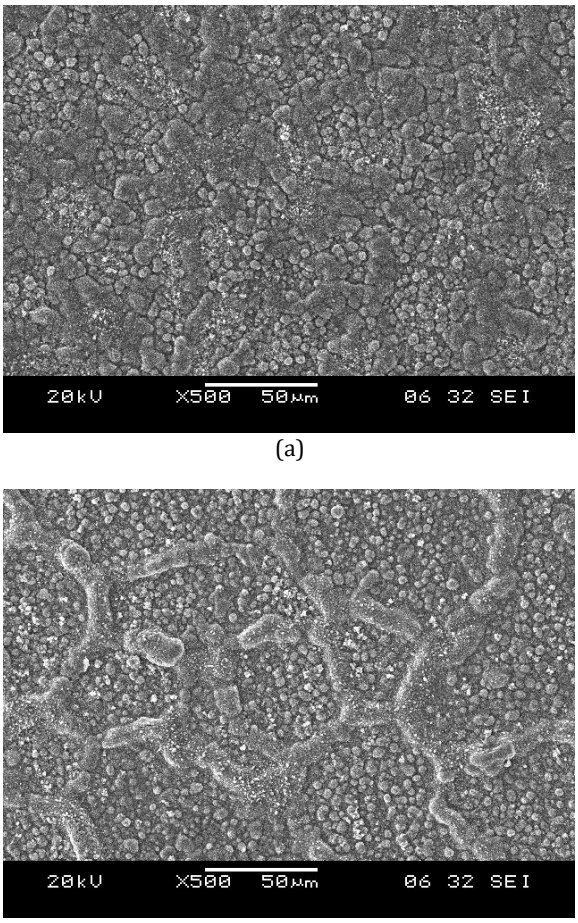

Figure 8. SEM images after isothermal oxidation for 100 hours: (a) LT950 and (b) HT1150 samples.

Figure 9 displays the SEM analysis of the fine-grained LT950 sample resulting from a 150 hour exposure. The image in Figure 9 (a) shows how several oxide styles combine to form an oxide scale with a uniform oxide structure. A close-up view at a high magnification of 10,000x analyzed in Figure 9 (b) shows a dense oxide structure has formed. This observation is consistent with the steady state condition in the oxidation kinetics of the LT950 sample after 150 hours exposure. Analysis of this fine-grained LT950 sample has shown that it follows a parabolic rate law. Exposure at 150 hours showed that this sample had reached a steady state where weight change was stable without dramatic weight gain.

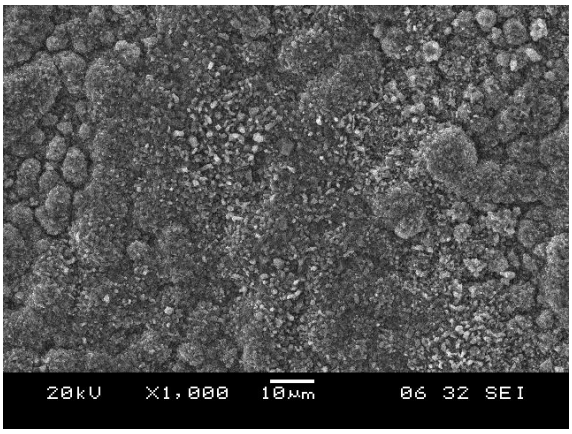

(a)

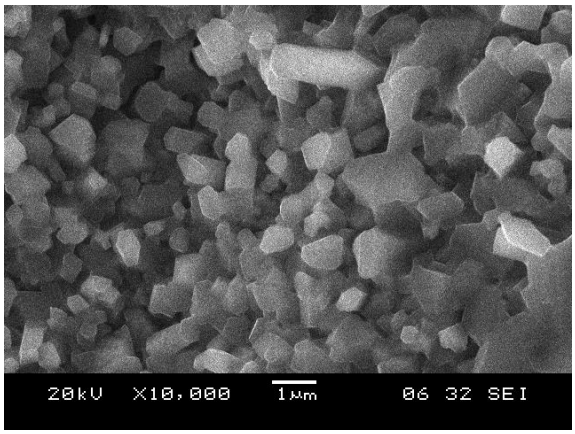

(b)

Figure 9. SEM images of LT9 50 samples after isothermal oxidation for 150 hours.

Figure 10 displays the SEM analysis of the coarse-grained HT1150 sample, with Figure 10 (a) and (b) displaying low magnification at 1,000x. The image in (a) shows the formation of cracks in the network-like structure that forms the grain boundary oxide. As previously shown in the SEM image after 100 hours, these oxides tend to have a higher oxidation rate due to high diffusion in the grain boundary short circuit region. In contrast, the image in (b) shows the co-formation of dense and porous oxide structures. The dense oxide structure has been highlighted in rectangular red lines with further analysis in a close-up view of higher magnification at 10,000x as shown in image (c) showing a spherical oxide-like structure. There is no evidence of cracks and voids occurring in this oxide area. Meanwhile, the porous oxide structure has been highlighted in rectangular blue lines and further analyzed in a close-up view in image (d), showing the formation of pores around the oxide. This observation indicates that the pores in the porous structure contribute to the extension of oxide formation. This is because the pores act as a pathway for the migration of oxygen ions towards the surface of the alloy to further develop the oxide scale. This phenomenon is consistent with the oxidation kinetics (Figure 1) of this coarse-grained HT1150 sample that records a higher weight gain and also obeys the liner rate law, indicating that continuous oxide scale will form as long as the alloy is exposed to high temperature conditions.

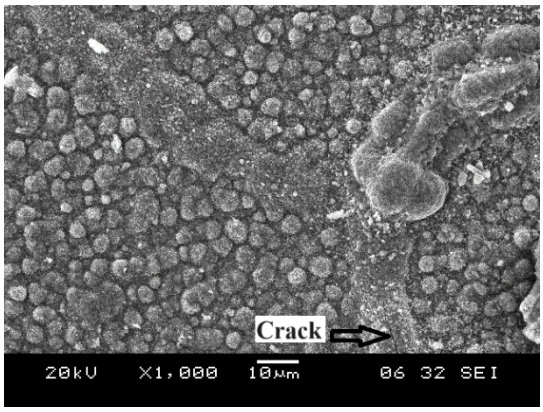

(a)

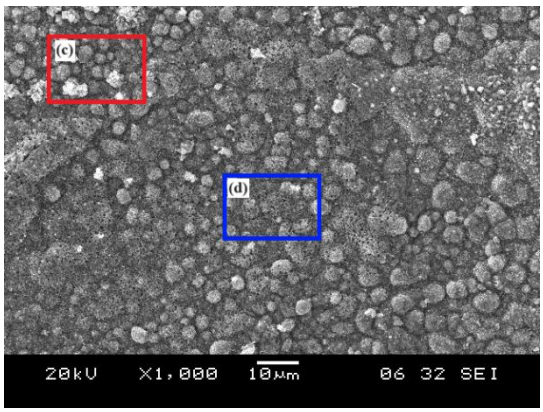

(b)

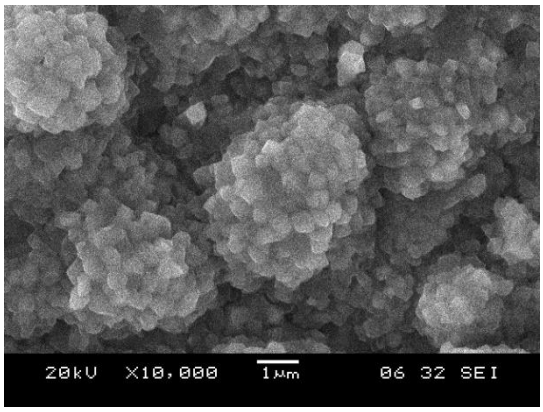

(c)

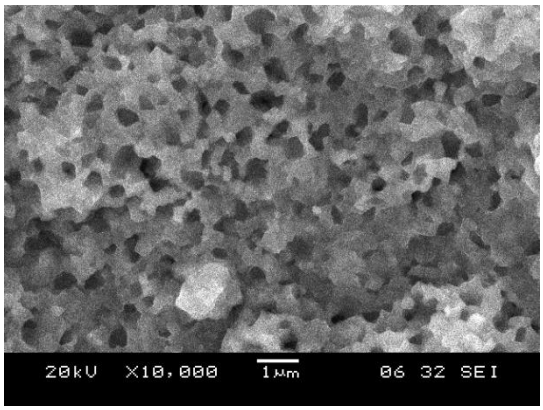

(d)

Figure 10 SEM images of HT11 50 samples after isothermal oxidation for 150 hours.

From our previous research [10], this linear rate law trend will slowly change to a parabolic rate law as the exposure period increases, when the oxide scale on the surface of the alloy reaches a protective property that begins to protect the base alloy form further oxidation process.

4. CONCLUSION

The heat treatment process successfully formed a fine-grained LT950 sample with grain size of 81.41 µm and hardness value of 81.04 HRB. Whereas, heat-treated HT1150 sample recorded a coarse-grained of 166.12 µm and a hardness value of 69.06 HRB. Isothermal oxidation tests on heat-treated LT950 and HT1150 were successfully studied. Fine-grained LT950 shows good results according to the lower parabolic rate constant of 1.79×10^{-6} $mg^2cm^{-4}s^{-1}$ indicating a low oxidation rate, thus good oxidation resistance. On the other hand, XRD analysis on LT950 sample detected the presence of Cr-containing oxides of the Cr_2O_3 and $MnCr_2O_4$ phases, with the addition of Ti-Cr oxide. These oxides will improve the protective behavior of the oxide scale that is formed. In conclusion, the fine-grained structure of the LT950 sample exhibits good oxidation resistance.

ACKNOWLEDGMENTS

The authors would like to acknowledge the Fundamental Research Grant Scheme (FRGS) of the Ministry of Higher Education Malaysia for its support, with grant number FRGS/1/2020/TK0/UNIMAP/02/43.

REFERENCES

[1] Wang, H., Liu, D., Wang, J., Shi, Y., Zheng, Y., Hu, Y. (2019). Investigation on the Thermal Deformation Behavior of the Nickel-Based Superalloy Strengthened by γ′ Phase. Crystals, Vol 9 (3), 125.

[2] Weber, J. H., Banerjee, M. K. (2016). Nickel-Based Superalloys: Alloying Reference Module in Materials Science and Materials Engineering. Elsevier: Amsterdam, The Netherlands.

[3] Zulnuraini, Z., Parimin, N. (2020). Isothermal oxidation behavior of Fe-33Ni-18Cr alloy in different heat treatment temperature. Materials Science Forum, Vol. 1010, 46–51.

[4] Shi, J., Zhang, T., Sun, B., Wang, B., Zhang, X., Song, L. (2020). Isothermal oxidation and TGO growth behavior of NiCoCrAlY-YSZ thermal barrier coatings on a Ni-based superalloy. Journal of Alloys and Compounds, Vol. 844,156093.

[5] Yang, J., Wang, S., Li, Y., Xu, D. (2020). Under-deposit corrosion of Ni-based alloy 825 and Fe-Ni based alloy 800 in supercritical water oxidation environment. Corrosion Science, Vol 167, 108493.

[6] Wang, Q., Pei, R., Liu, S., Wang, S., Dong, L., Zhou, L., Xi, Y., Bai, S. (2020). Microstructure and corrosion behavior of different clad zones in multi-track Ni-based laser-clad coating. Surface and Coating Technology, Vol. 402, 126310.

[7] Oquab, D., Xu, N., Monceau, D., Young, D. J. (2010). Subsurface Microstructural Changes in a Cast Heat Resisting Alloy Caused by High Temperature Corrosion. Corrosion Science, Vol. 52, 255–262.

[8] Zurek, J., Young, D. J., Essuman, E., Hänsel, M., Penkalla, H.J., Niewolak, L., Quadakkers, W.J. (2008). Growth and Adherence of Chromia Based Surface Scales on Ni-Base Alloys in High- and Low-pO2 Gases. Materials Science and Engineering: A, Vol. 477 (1-2), 259–270.

[9] Tan, L., Ren, X., Sridharan, K. and Allen, T. R. (2008). Effect of Shot-Peening on the Oxidation of Alloy 800H Exposed to Supercritical Water and Cyclic Oxidation. Corrosion Science, Vol. 50 (7), 2040–2046.

[10] Parimin, N., Hamzah, E. (2022). Influence of Ti on Oxide Formation During Isothermal Oxidation of 800H Ni-Based Alloys. Key Engineering Materials, Vol. 929, 29-34.

[11] Zhang, J. F., Tu, Y. F., Xu, J., Zhang, J. S., Zhang, J. L. (2008). Effect of Solid Solution Treatment on Microstructure of Fe-Ni Based High Strength Low Thermal Expansion Alloy. Iron and Steel Research, International, Vol. 15, 75–78.

[12] Cai, D., Mei, Y., Pulin, N. and Wenchang, L. (2003). Influence of Solution Treatment Temperature on Mechanical Properties of a Fe–Ni–Cr Alloy. Materials Letters, Vol. 57 (24-25), 3805–3809.

[13] Parimin, N., Hamzah, E. (2020). Effect of Solution Treatment Temperature on the Microstructure of Fe-33Ni-19Cr Alloy. MaterialsScience Forum, Vol. 1010, 21-27.

[14] Holcomb, G. R., Alman, D. E. (2006). The Effect of Manganese Additions on the Reactive Evaporation of Chromium in Ni–Cr Alloys. Scripta Materialia, Vol. 54, 1821-1825.